X-RAY TOMOGRAPHY BASED FINITE ELEMENT MODELLING OF NON-CRIMP FABRIC BASED FIBRE COMPOSITE

Kristine M. Jespersen*[1,2,3], Leif E. Asp[4], Atsushi Hosoi[2], Hiroyuki Kawada[2], Lars P. Mikkelsen[1]

[1]Department of Wind Energy, Section of Composites and Materials Mechanics, Technical University of Denmark, Risø Campus, Roskilde, Denmark (Email: kmun@dtu.dk*)
[2]Department of Applied Mechanics and Aerospace Engineering, Waseda University, Tokyo, Japan
[3]Kanagawa Institute of Industrial Science and Technology (KISTEC), Kanagawa, Japan
[4]Industrial & Materials Science Department, Chalmers University of Technology, Gothenburg, Sweden

Keywords: Micro-tomography, Glass fibre reinforced polymer, Finite element method, Fibre bundle structure,

Abstract
The current study presents a workflow to import a fibre bundle structure of a non-crimp fabric based fibre composite obtained by X-ray CT to a solvable 3D model in the finite element software ABAQUS. The considered fibre composite is similar to that used for the load carrying parts of wind turbine blades, and each layer of the non-crimp fabric contains fibre bundles oriented in the 0°, 90°, and ±45° directions. The 3D fibre bundle geometry is first segmented in the software AVIZO and then imported to Geomagic Wrap where the geometry is smoothened and converted into a nurbs surface that can be imported into ABAQUS. The resulting stress distribution is qualitatively compared to previous experimental observations and discussed.

1. Introduction

Due to their high specific stiffness and strength along with high toughness and great fatigue properties fibre composites are increasingly replacing the more conventional materials such as steel and aluminium. Particularly within the wind, automotive and aerospace industries fibre composites are increasingly being used for structural parts. For such applications it is important to understand the behaviour of the material under various loading conditions to make sure the parts do not fail prematurely. However, at the same time it is important not to heavily over-dimension the structure, as it will increase the cost. In the case of wind turbines, the main spars in the blades that mainly carry the gravitational and wind loads are made from uni-directional (UD) non-crimp fabric (NCF) based fibre composites and experience a high number of fatigue load cycles during the blade life-time of around 20-30 years. The current methods for determining the life-time of these materials are based on approaches adopted from metals despite the damage mechanisms of observed fibre composite under fatigue loading (e.g. [1–3]) being considerably different. The UD NCF based fibre composites used for wind turbine blades experience complex damage mechanisms during fatigue loading [4–7], which is highly dependent on the local variation of the fibre bundle structure [8]. Therefore, it is important to establish modelling methods able to take into account the actual fibre and bundle structure to ensure realistic results.

One possible way to model the actual fibre bundle structure in 3D is to extract the 3D structure from X-ray computed tomography (CT) images and carry out finite element modelling (FEM) using the extracted geometry (X-ray CT based modelling). Although few, studies have been carried out on this subject

both on the fibre [9, 10] and bundle [11–17] scales. Naouar et al. considered a 2D [12] and 3D [13] woven fibre composite and used various image analysis techniques based on the structure tensor and a homogenisation parameter, respectively, to segment the fibre bundles. It was found that the established model using the real fibre bundle structure gave results closer to experiments than a model using a perfect pattern generated by TexGen [12]. Although carried out for woven fabrics rather than UD NCFs considered in the present study, these studies also confirm the importance of considering the actual bundle structure as highlighted by the authors and others through experimental studies [4–6, 8, 18]. Nevertheless, there are cases where automatic segmentation approaches will not work well or where it is useful to compare the results obtained by automatic approaches to other methods. Particularly for the considered material, the fibre bundles are touching one another making them challenging to separate. Thus, the current study presents one possible approach to successfully transfer a 3D X-ray geometry to a solvable ABAQUS model by means of commercially available software. The main focus of the current work is on the approach itself, however the stress distribution obtained by modelling the real fibre bundle structure by the presented approach is also shown and qualitatively compared to experiments.

2. Material and methods

2.1. Composite material

The considered material is a UD NCF based fibre composite commonly used for the main load carrying parts of wind turbine blades, similar to that used in [6]. This type of fibre composite consists of layers of non-crimp fabrics made up from fibre bundles mainly oriented in the direction of the load, but with around 10% differently oriented (off-axis) supporting backing fibre bundles present. Fig. 1a shows a schematic of one layer of fabric. For further details on the material system, the reader is referred to [6], where the same material is explained in greater detail. Fig. 1b shows an example of UD fibre fractures observed at a cross-over region of the backing fibre bundles touching a UD fibre bundle. This type of region is considered as being critical for damage initiation and progression [6, 18], as will also be discussed in he results section.

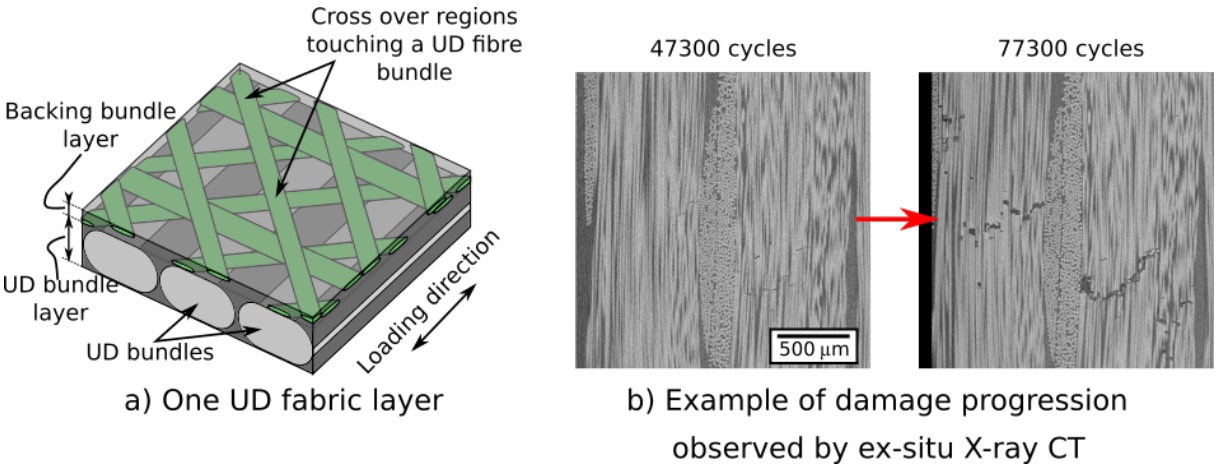

Figure 1. Schematic of (a) structure of one layer of UD fabric and (b) UD fibre fracture accumulation during fatigue loading near a contacting cross-over region of the fibre bundles [6].

2.2. X-ray computed tomography

To obtain the actual fibre bundle structure present inside the composite material, X-ray CT experiments were carried out. The experiments were carried out on a Zeiss Xradia Versa 520 at 60kV with a source-to-sample distance of 26mm and a detector-to-sample distance of 150mm resulting in a field of view (FoV)

of around 10x10x10mm. The size of the detector was 2000x2000 pixels with 0.4x optical magnification and the experiments were carried out with a binning of 2 resulting in a pixel size of ~10μm. The number of projections were 3201 and the exposure time was 3.5s resulting in an approximate scan time of ~4.5h. Although it is desirable to consider as large a region as possible, the image resolution decreases with increasing FoV size and it is therefore a compromise. In the current case, a FoV of 10x10x10mm was chosen to have sufficient resolution to visually distinguish between the different fibre bundles while still considering a relatively large region. Data conversion and visualisation was done in AVIZO 9.0.0 by FEI.

2.3. Segmentation and modelling method

In this section the steps that are part of the overall workflow of getting from the X-ray CT data to the finite element model are explained. In the current study, focus has been on using commercial software and it was chosen to use AVIZO, Geomagic Wrap, and ABAQUS. Fig. 2 illustrates the steps of the established workflow that will be explained in more detail in the following sections.

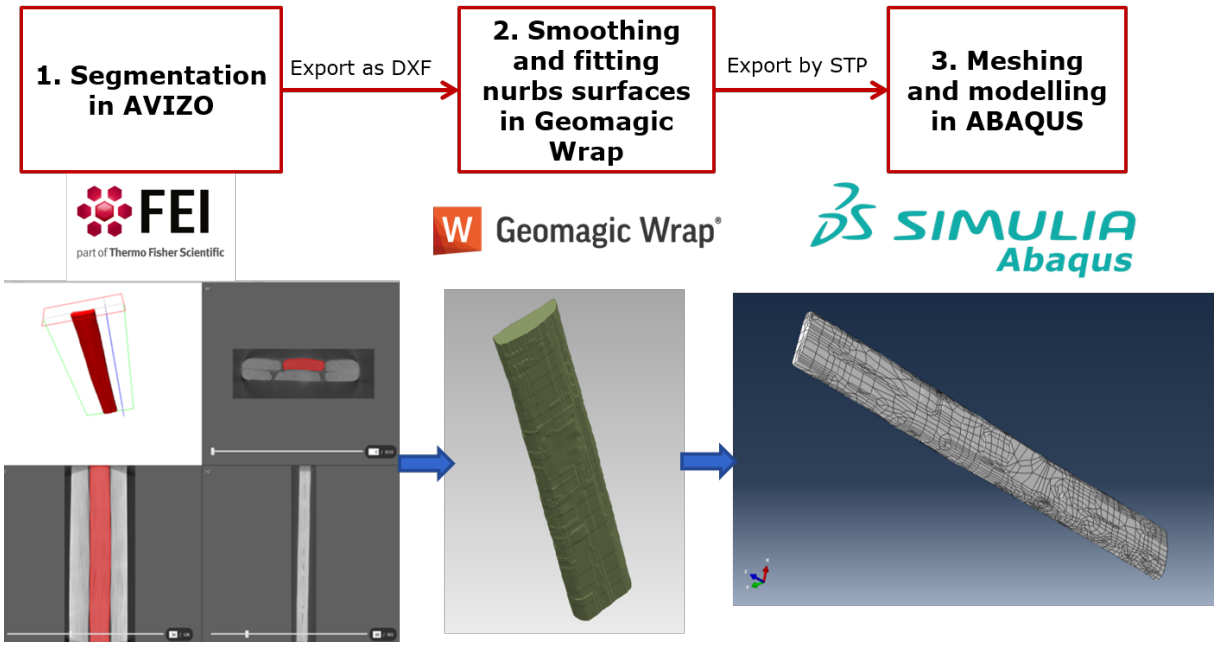

Figure 2. Workflow for getting from the X-ray CT data to an ABAQUS model

2.3.1. Fibre bundle segmentation in AVIZO

The first step is to segment the fibre bundles. In other words, to place a colour mask on top of the relevant parts of the image representing each of the regions one wants to separate from one another. In this case, we want to separate the fibre bundles from the matrix and the fibre bundles oriented in different directions from one another. This was done by slicing through the volume in AVIZO and for each bundle manually painting on top of the cross section in some of the slices. As painting in every single slice would not be feasible time-wise, this was only done for a number of slices and then AVIZO was used to interpolate between the marked regions. This is also illustrated in Fig. 3.

The regions where the backing fibre bundles and the UD fibre bundles touch one another have been found to be significantly more critical [4–6, 8, 18] than the contact between two UD bundles. Therefore, the backing fibre bundles were segmented individually, whereas the UD fibre bundles were segmented layer-by-layer. If necessary, it would also be possible to segment all fibre bundles individually. A video

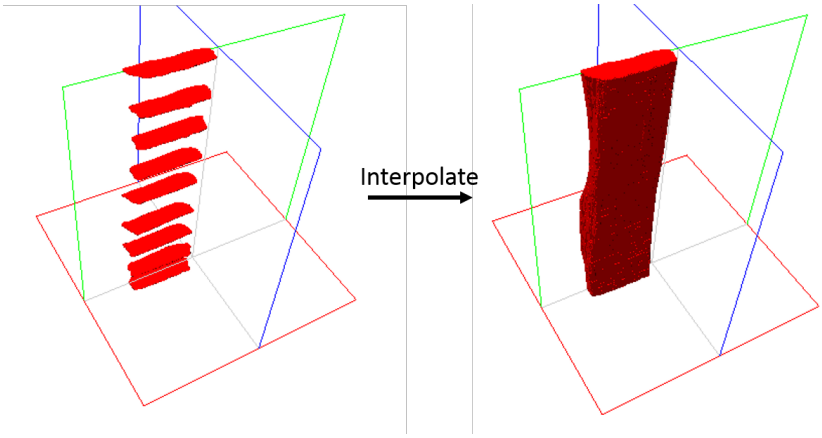

Figure 3. Example of interpolation between segmented slices of fibre bundle in AVIZO

demonstrating the final segmentation can be found online [19]. To export the segmented data, surfaces were generated for each backing layer direction (+45, -45, 90) and each UD layer, where after each surface could be exported in the DXF format. This format was chosen since other surface formats such as STL provided surfaces with holes at contacting regions. Details on how to do so in AVIZO can be found as supplementary material available online [19].

2.3.2. Smoothing and conversion in Geomagic Wrap

One way convert the segmented data into a type importable to ABAQUS is to use the software Geomagic Wrap as an intermediate step. Geomagic Wrap allows to smoothen and repair the surfaces and then fit a grid of nurbs surface patches to the surface. The overall workflow for fitting nurbs surfaces to the geometry is demonstrated in Fig. 4. This step may require some additional manual work to make the surface fit work properly depending on the complexity of the surface. In the case of the fibre bundles it was necessary to create some partitions and do some final adjustments to the patches manually. More details on how to import the DXF surfaces, fit nurbs surfaces, and export to STP for import in ABAQUS can be found as supplementary material online [19].

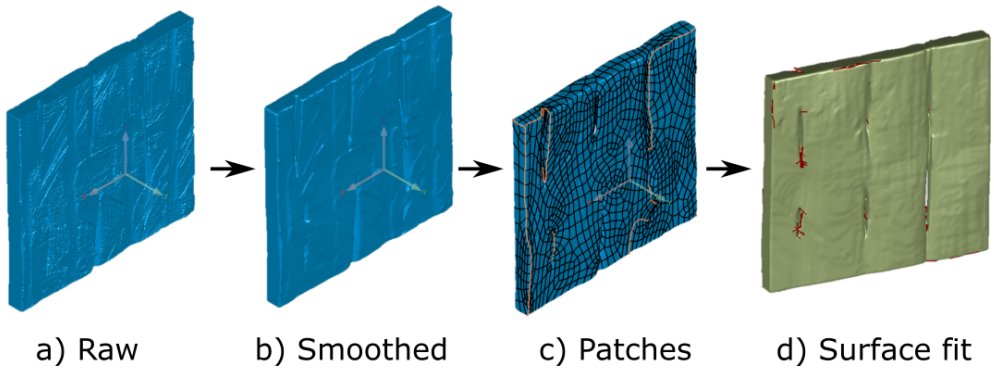

Figure 4. Example of workflow in Geomagic Wrap

2.3.3. Import of geometry and modelling in ABAQUS

The created STP files for each UD bundle layer and each direction of the backing fibre bundles were imported to ABAQUS as separate parts. Fig. 5 shows a schematic of the overall workflow in ABAQUS. In the current study, the meshing refining was done by edge seeds as patches generated in Geomagic

Wrap becomes surfaces connected by edges when imported into ABAQUS (see Fig. 5a). Thus, the refined mesh regions are already defined when the patches were generated in the Geomagic Wrap step. However, it would be possible to remesh the geometry subsequently in ABAQUS as well if desired. Quadratic tetrahedral elements (C3D10) were used for the current model, and the mesh for the fibre bundles and the matrix block can be seen in Fig. 5b and 5c, respectively. The total number of elements for the model was 174331.

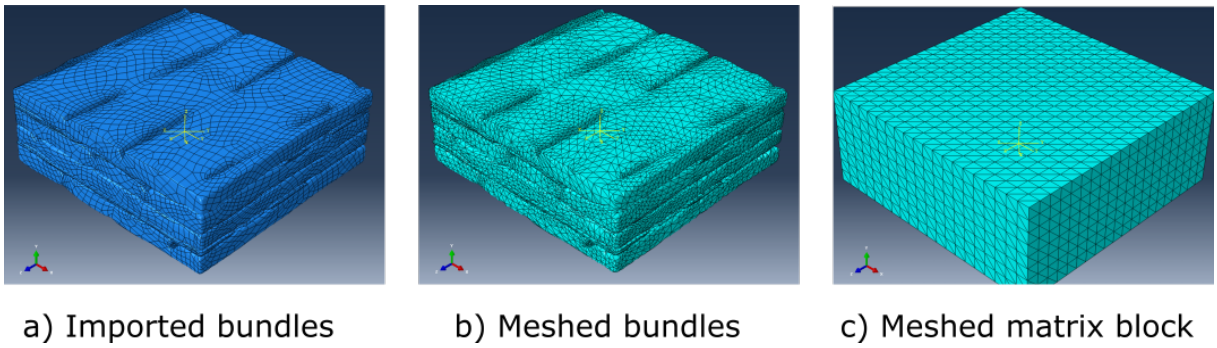

Figure 5. Example of workflow in ABAQUS

The FEM analysis was carried out with the material properties of $E_m = 3.3$ MPa, $\nu_m = 0.3$ for the matrix and $E_1 = 30$ GPa, $E_2 = E_3 = 9.8$ GPa, $G_{12} = G_{13} = G_{23} = 2.8$ GPa, $\nu = 0.3$ for the fibre bundles. All the materials were assumed to be linear elastic. Local coordinate systems were used to align the stiffness direction of the fibre bundles into their respective overall fibre orientation directions (0°, 90° and ±45°) with E_1 in the length direction. It would be possible to obtain more precise material properties for the fibre bundles by measuring the fibre volume fraction inside the fibre bundles and using the rule of mixtures, however this has not been done in the current study. The fibre bundles were modelled as an embedded region into a block of matrix. The matrix block was fixed in one end and a displacement load of 0.1% strain was applied to the other resulting in uni-axial loading in the 0° direction.

3. Results

Fig. 6 shows the stresses in the axial direction where the matrix has been hidden for clarity. Some edge effects can be seen in the ends of the UD fibre bundles as a result of the boundary conditions (load induced on the surrounding matrix block). However, the stresses in the UD fibre bundles are seen to quickly stabilise when moving away from the edges. Fig. 7a and 7b shows the stress state with the top UD bundle layer removed, with and without the backing layer, respectively. It can be seen from Fig. 7a that the stresses locally are higher in a band across the UD fibre bundles. The location of this band correlate well with the location of the backing fibre bundles (Fig. 7b). Hence, the presence of the backing fibre bundle seems to locally affect the stress state in the UD fibre bundles even for the simple uniaxial tension load case considered in the current study. As discussed earlier, fractures of the load carrying UD fibres observed during fatigue loading has been experimentally shown to initiate locally close to the intersecting regions of the supporting backing fibre bundles and a UD bundle. The locally higher stresses seen in Fig. 7a could be part of the explanation of why the fatigue damage initiate and progress in these regions.

In addition to the edge effects induced by the load application approach, edge effects are also observed in the width direction as marked by arrows in Fig. 7a. Due to the resolution limitations, the considered volume (10mm^3 does not include the full width of the test specimen (15mm). Therefore, the stresses at the edges seen in Fig. 7 will not be exactly the same as in if the test specimen was subjected to tensile loading. It is also seen that although a relatively large region is considered, it is not large enough to

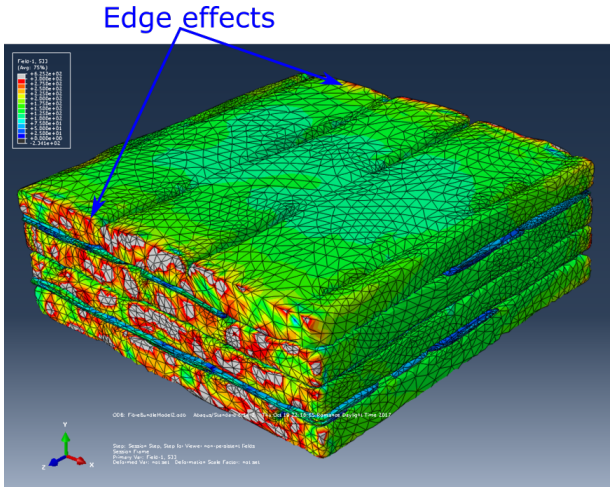

Figure 6. Axial stress distribution of the full volume (matrix hidden)

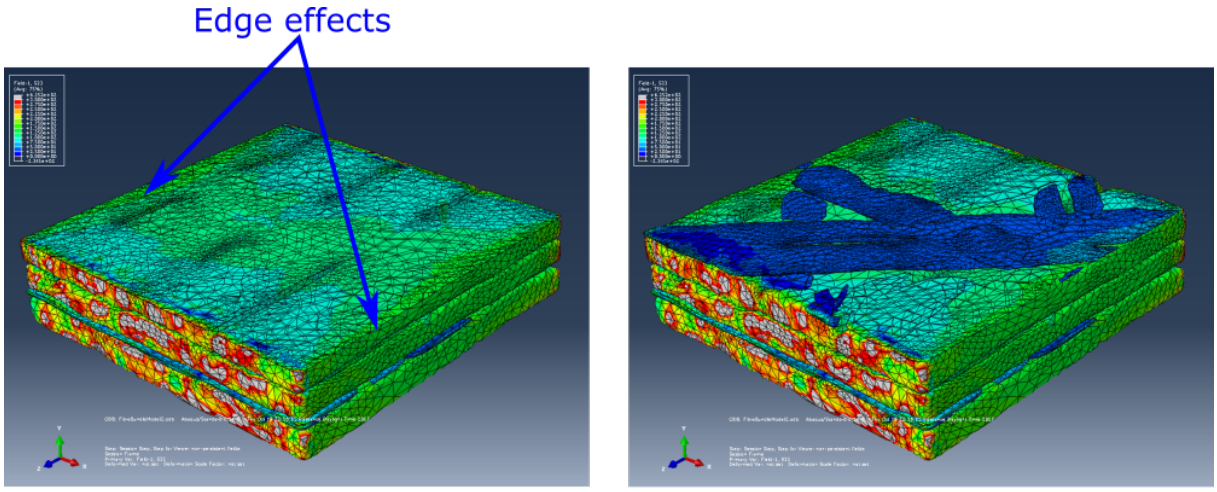

Figure 7. Stress distributions showing the local effect of the backing fibre bundles

be representative of the backing bundle structure. These considerations highlights the importance of considering a significantly large volume if the model should be representative as part of a multi-scale model approach.

In principle, it would be possible to stitch together several X-ray CT data-sets both in the axial and width directions to obtain a larger volume at the same resolution. However, using the current approach the number of elements will become too high and the time necessary for manual segmentation and surface fitting work will become unfeasible. Therefore, there is a future need to establish automatic segmentation and meshing method to extract these fibre bundle structures from X-ray CT data. Aside from saving time on manual work, automatic methods would also eliminate the personal bias introduced by manually choosing the regions belonging to each fibre bundle. In relation to the model becoming increasingly heavy when considering a larger volume, automatic segmentation methods are likely to make it easier to create a more effective mesh e.g. by sweeping the mesh along the fibre directions and locally refine the mesh at sensitive regions (see also Blinzler et al.[20]). Nevertheless, the current work serves as a good

starting point and comparison base for future improved approaches for X-ray CT based modelling and used a free segmentation making it applicable to most geometries. For additional future work, it would be interesting to include contact between the fibre bundles and the local fibre orientation as part of the material properties in the analysis.

4. Conclusions

The present study presented an approach to import a fibre bundle structure of a composite material from 3D X-ray CT data into the finite element software ABAQUS. The stress distribution with a main focus on stress concentration areas was qualitatively compared to experimental observations of previous studies, and the stress concentrations were found to be in accordance to locations of load carrying fibre fracture initiation. The presented approach has a high degree of freedom as it can apply to most geometry types, however as it is quite time consuming and based on subjective judgment, there is a future need for automatic segmentation and import workflows to be developed.

Acknowledgments

Financial supported from MAX4ESSFUN a European Union inter-regional Cross Border Network and Researcher Programme is acknowledged. This research was conducted using mechanical testing equipment from DTU Center for Advanced Structural and Material Testing (CASMAT), Grant No. VKR023193 from Villum Fonden.

References

[1] K. L. Reifsnider and R. Jamison. Fracture of fatigue-loaded composite laminates. *International Journal of Fatigue*, 4(4):187–197, 1982.

[2] R. D. Jamison, K. Schulte, K. L. Reifsnider, and W. W. Stinchcomb. Characterization and analysis of damage mechanisms in tension-tension fatigue of graphite/epoxy laminates. *Effects of Defects in Composite Materials*, STP30196S:21–55, 1984.

[3] R. Talreja. Fatigue of composite materials: damage mechanisms and fatigue-life diagrams. *Proceedings of the Royal Society A*, 378:461–475, 1981.

[4] J. Zangenberg, P. Brøndsted, and J. W. Gillespie Jr. Fatigue damage propagation in unidirectional glass fibre reinforced composites made of a non-crimp fabric. *Journal of Composite Materials*, 48(22):2711–2727, 2014.

[5] K. M. Jespersen, J. Zangenberg, T. Lowe, P. J. Withers, and L. P. Mikkelsen. Fatigue damage assessment of uni-directional non-crimp fabric reinforced polyester composite using X-ray computed tomography. *Composites Science and Technology*, 136:94–103, 2016.

[6] Kristine M. Jespersen and Lars P. Mikkelsen. Three dimensional fatigue damage evolution in non-crimp glass fibre fabric based composites used for wind turbine blades. *Composites Science and Technology*, 153:261–272, 2017.

[7] K. Vallons, G. Adolphs, P. Lucas, S. V. Lomov, and I. Verpoest. The influence of the stitching pattern on the internal geometry, quasi-static and fatigue mechanical properties of glass fibre non-crimp fabric composites. *Composites: Part A*, 56:272–279, 2014.

[8] K. M. Jespersen, J. A. Glud, J. Zangenberg, A. Hosoi, H. Kawada, and L. P. Mikkelsen. Uncovering the fatigue damage initiation and progression in uni-directional non-crimp fabric reinforced polyester composite. *Composites Part A: Applied Science and Manufacturing*, 2018.

[9] M. J. Emerson, K. M. Jespersen, A. B. Dahl, K. Conradsen, and L. P. Mikkelsen. Individual fibre segmentation from 3D X-ray computed tomography for characterising the fibre orientation in unidirectional composite materials. *Composites Part A: Applied Science and Manufacturing*, 97:83–92, jun 2017.

[10] M. W. Czabaj, M. L. Riccio, and W. W. Whitacre. Numerical reconstruction of graphite/epoxy composite microstructure based on sub-micron resolution X-ray computed tomography. *Composites Science and Technology*, 105:174–182, 2014.

[11] M. N. Saleh, G. Lubineau, P. Potluri, P. J. Withers, and C. Soutis. Micro-mechanics based damage mechanics for 3D orthogonal woven composites: Experiment and numerical modelling. *Composite Structures*, 156:115–124, 2016.

[12] N. Naouar, E. Vidal-Sallé, J. Schneider, E. Maire, and P. Boisse. Meso-scale FE analyses of textile composite reinforcement deformation based on X-ray computed tomography. *Composite Structures*, 116(1):165–176, 2014.

[13] N. Naouar, E. Vidal-Salle, J. Schneider, E. Maire, and P. Boisse. 3D composite reinforcement meso F.E. analyses based on X-ray computed tomography. *Composite Structures*, 132:1094–1104, 2015.

[14] Y. Li, B. Sun, and B. Gu. Impact shear damage characterizations of 3D braided composite with X-ray micro-computed tomography and numerical methodologies. *Composite Structures*, 176:43–54, 2017.

[15] D. S. Mikhaluk, T. C. Truong, A. I. Borovkov, S. V. Lomov, and I. Verpoest. Experimental observations and finite element modelling of damage initiation and evolution in carbon/epoxy non-crimp fabric composites. *Engineering Fracture Mechanics*, 75(9):2751–2766, 2008.

[16] S. Topal, L. Baiocchi, A. D. Crocombe, S. L. Ogin, P. Potluri, P. J. Withers, M. Quaresimin, P. A. Smith, M. C. Poole, and A. E. Bogdanovich. Late-stage fatigue damage in a 3D orthogonal non-crimp woven composite: An experimental and numerical study. *Composites Part A: Applied Science and Manufacturing*, 79:155–163, 2015.

[17] L. P. Djukic, G. M. Pearce, I. Herszberg, M. K. Bannister, and D. H. Mollenhauer. Contrast enhancement of microCT scans to aid 3D modelling of carbon fibre fabric composites. *Applied Composite Materials*, 20(6):1215–1230, 2013.

[18] K. M. Jespersen and L. P. Mikkelsen. Fatigue damage observed non-destructively in fibre composite coupon test specimens by X-ray CT. *IOP Conference Series: Materials Science and Engineering*, 139:012024, 2016.

[19] K. M. Jespersen and L. P. Mikkelsen. X-ray CT based FEM model data of non-crimp fabric based fibre composite [Data set]. `https://doi.org/10.5281/zenodo.1244332`, 2018.

[20] B. J. Blinzler, D. Wilhelsson, L. E. Asp, K. M. Jespersen, and L. P. Mikkelsen. A systematic approach to transforming composite 3d images into meso-scale computational models. *18th European Conference on Composite Materials*, (June), 2018.